AIP | Journal of Applied Physics

An effective approach for the minimization of errors in capacitance-voltage carrier profiling of quantum structures

Dipankar Biswas and Siddhartha Panda

Citation: Journal of Applied Physics **115**, 134308 (2014); doi: 10.1063/1.4870287
View online: http://dx.doi.org/10.1063/1.4870287
View Table of Contents: http://scitation.aip.org/content/aip/journal/jap/115/13?ver=pdfcov
Published by the AIP Publishing

An effective approach for the minimization of errors in capacitance-voltage carrier profiling of quantum structures

Dipankar Biswas[a] and Siddhartha Panda
Institute of Radiophysics and Electronics, University of Calcutta, 92 A. P. C. Road, Kolkata 700009, India

(Received 6 September 2013; accepted 21 March 2014; published online 2 April 2014)

Experimental capacitance–voltage (*C-V*) profiling of semiconductor heterojunctions and quantum wells has remained ever important and relevant. The apparent carrier distributions (ACDs) thus obtained reveal the carrier depletions, carrier peaks and their positions, in and around the quantum structures. Inevitable errors, encountered in such measurements, are the deviations of the peak concentrations of the ACDs and their positions, from the actual carrier peaks obtained from quantum mechanical computations with the fundamental parameters. In spite of the very wide use of the *C-V* method, comprehensive discussions on the qualitative and quantitative nature of the errors remain wanting. The errors are dependent on the fundamental parameters, the temperature of measurements, the Debye length, and the series resistance. In this paper, the errors have been studied with doping concentration, band offset, and temperature. From this study, a rough estimate may be drawn about the error. It is seen that the error in the position of the ACD peak decreases at higher doping, higher band offset, and lower temperature, whereas the error in the peak concentration changes in a strange fashion. A completely new method is introduced, for derivation of the carrier profiles from *C-V* measurements on quantum structures to minimize errors which are inevitable in the conventional formulation. © *2014 AIP Publishing LLC*. [http://dx.doi.org/10.1063/1.4870287]

I. INTRODUCTION

With the advent of new materials and applications, semiconductors heterojunctions and quantum wells (QWs) are being progressively used in the area of optoelectronic devices like laser diodes, LEDs, photodetectors, solar cells, high electron mobility transistors, heterojunction field effect transistors, and so on.[1–7] The major issues of characterization of such devices are the band offset of the heterojunction, carrier accumulation and distribution, presence of interface states, traps, and deep levels, position of the interface, etc. The most convenient and widely used techniques for such characterizations of nanostructures are the capacitance-voltage (*C-V*) measurement and its different forms, deep level transient spectroscopy, etc.[8–15] In spite of the wide use of the *C-V* profiling for the last couple of decades, several aspects of the process remain unexplored. Recently, we have highlighted proper design of nanostructures for *C-V* measurements[16] and we have explained the nature of temperature shifts of *C-V* carrier profiles.[17] Further to this, we have explained the different shift of carrier peaks in normal and inverted heterostructures.[18]

The carrier distribution, obtained from the *C-V* measurement, is generally called *C-V* carrier profile or apparent carrier distribution (ACD). In the case of heterojunctions and QWs, ACDs are significantly different from the actual carrier distributions, calculated from the fundamental parameters through quantum mechanical computations.[19] These are different from the bulk semiconductors as well. Thus, the measured carrier profile introduces tangible errors from the actual profile, which depends on the fundamental parameters and the temperature of the measurements.

The typical structures and the band diagrams for the *C-V* measurement are available in the literature.[13,15] The ACDs and actual carrier distributions for QW structures are well discussed in the literature[15,19] but the carrier distributions in and around heterojunctions for different parameters including quantum mechanical calculations are not readily available. Moreover, in spite of numerous research reports on the *C-V* profiling of such nanostructures, minimization of errors in the measurements has not been well discussed or addressed.

In this paper, we have made rigorous calculations to find the carrier distribution in and around a heterojunction with the fundamental parameters, results of which are presented with suitable discussions. The aim of this work is to reduce the error in the measurement for better accuracy.

For our studies, we have considered normal n-type heterojunctions of GaAs/$Al_xGa_{1-x}As$ which is a commonly used lattice matched hetero-pair. The actual carrier profiles in the structures have been computed through self-consistent solutions of the Schrödinger and Poisson equations. The ACDs have been determined from the calculated capacitances of the structures.

The conventional formulation for the extraction of the carrier distribution from experimental *C-V* data produces significant errors in the ACD.[17,18] In this paper, we introduce a new method for computation of carrier profile from measured *C-V* data, which is much more accurate and fits the actual carrier distribution much better.

Errors arising from the series resistance during measurements are briefly highlighted.

II. THEORETICAL DETAILS

In our calculations, we consider n-type GaAs/$Al_xGa_{1-x}As$ heterojunctions with Al Schottky on $Al_xGa_{1-x}As$. In a

[a]Electronic mail: diiibiswas@yahoo.co.in

heterojunction, the triangular QW which arises due to the accumulation of carriers is described by the potential energy[20]

$$V(z) = -q\varphi(z) + \Delta E_c(z), \tag{1}$$

where ΔE_c is the band offset of the conduction band and φ is the electrostatic potential, determined by the ionized donor concentration, $N_D{}^+$ and electron concentration n through the Poisson equation,

$$\frac{d}{dz}\left(\varepsilon(z)\frac{d\varphi(z)}{dz}\right) = -q\left[N_D^+(z) - n(z)\right]. \tag{2}$$

The electron concentration in the QW, again, depends on the quantized energy states and the wave functions of the electrons, which are obtained from the Schrödinger equation,

$$-\frac{\hbar^2}{2}\frac{d}{dz}\left(\frac{1}{m^*(z)}\frac{d\psi(z)}{dz}\right) + V(z)\psi(z) = E\psi(z). \tag{3}$$

It is found that the parameters involved in the Schrödinger and Poisson equations are mutually dependent, which give rise to the necessity of the self-consistent solution of the two equations to determine the electron distributions in the structures. To solve the two equations self-consistently, Eqs. (2) and (3) are discretized using finite difference method with non-uniform mesh as[20]

$$\left(\frac{2\varepsilon_{i+1/2}(\varphi_{i+1} - \varphi_i)}{h_i(h_i + h_{i-1})} - \frac{2\varepsilon_{i-1/2}(\varphi_i - \varphi_{i-1})}{h_{i-1}(h_i + h_{i-1})}\right) + q\left(N_{Di}^+ - n_i\right) = 0 \tag{4}$$

and

$$-\frac{\hbar^2}{2}\left(\frac{2(\psi_{i+1} - \psi_i)}{m^*_{i+1/2}h_i(h_i + h_{i-1})} - \frac{2(\psi_i - \psi_{i-1})}{m^*_{i-1/2}h_{i-1}(h_i + h_{i-1})}\right) + V_i\psi_i = E\psi_i, \tag{5}$$

respectively, where h_i is the mesh size between adjacent grid points z_{i+1} and z_i. Equation (4) is solved by Newton-Raphson method using the matrix equation,[21]

$$J\delta\varphi = -f\left(\varphi^0\right), \tag{6}$$

where J is the Jacobian matrix expressed as

$$J_{ij} = \begin{cases} \dfrac{2\varepsilon_{i+1/2}}{h_i(h_i + h_{i-1})} & \text{if } j = i+1, \\ \dfrac{2\varepsilon_{i-1/2}}{h_{i-1}(h_i + h_{i-1})} & \text{if } j = i-1, \\ -J_{ii-1} - J_{ii+1} + q\dfrac{\partial\left(N_{Di}^+ - n_i\right)}{\partial\varphi_i} & \text{if } j = i, \\ 0 & \text{otherwise,} \end{cases} \tag{7}$$

$\delta\varphi$ is the correction vector to the initial approximation vector φ^0 to obtain the actual vector φ as

$$\varphi = \varphi^0 + \delta\varphi, \tag{8}$$

and f is given by

$$f_i = \left(\frac{2\varepsilon_{i+1/2}(\varphi_{i+1} - \varphi_i)}{h_i(h_i + h_{i-1})} - \frac{2\varepsilon_{i-1/2}(\varphi_i - \varphi_{i-1})}{h_{i-1}(h_i + h_{i-1})}\right) + q\left(N_{Di}^+ - n_i\right). \tag{9}$$

In each iteration of the Newton-Raphson method, Eq. (5) is solved to provide the term n_i. By this, the self-consistency of the two equations is achieved. To solve Eq. (5), it is transformed to a matrix eigenvalue equation as

$$H\psi = E\psi, \tag{10}$$

where H is a tri-diagonal matrix given by

$$H_{ij} = \begin{cases} -\dfrac{\hbar^2}{2}\left(\dfrac{2}{m^*_{i+1/2}h_i(h_i + h_{i-1})}\right) & \text{if } j = i+1, \\ -\dfrac{\hbar^2}{2}\left(\dfrac{2}{m^*_{i-1/2}h_{i-1}(h_i + h_{i-1})}\right) & \text{if } j = i-1, \\ -H_{ii+1} - H_{ii-1} + V_i & \text{if } j = i, \\ 0 & \text{otherwise.} \end{cases} \tag{11}$$

A standard matrix eigenvalue solver routine has been developed to solve Eq. (10).

The boundary conditions for the Poisson equation are, at the surface φ is equal to the Schottky barrier height and in the neutral region, far away from the Schottky, φ is equal to the potential corresponding to the energy of the conduction band edge. The second boundary condition is computed taking into account the splitting of the Fermi level due to the applied bias, conduction band offset, and donor concentration in GaAs. It appears that the boundary conditions set $V(z)$ equal to the energy of the conduction band edge considering the equilibrium Fermi level as the reference.

To determine the electron concentration, we have considered both the quantum states in the QW and the continuum states above these.[22]

To determine the C-V characteristics, the capacitance of the structure for an applied bias is computed from the change of the surface electric field due to the small change of the applied bias using Gauss theorem.[15] The ACD in the structure is obtained from this calculated C-V data through the formulation of the C-V technique.[18]

Parameters of GaAs/$Al_xGa_{1-x}As$ structures, used in the calculations, are given in Table I. The donor ionization energies of Si dopants in GaAs and AlGaAs are 5 meV (Ref. 15) and 50 meV (Ref. 23), respectively, which have a significant effect on the carrier concentration especially at low temperature.

III. RESULTS AND DISCUSSION

Fig. 1 shows ACDs in the GaAs/$Al_{0.3}Ga_{0.7}As$ heterojunctions at the temperature 300 K for different doping levels (N_{DH}) in the higher band gap material, i.e., in AlGaAs over a wide range. ACDs at 50 K are also depicted in the figure for two different values of N_{DH} to observe the temperature

TABLE I. Parameters used for the simulation on GaAs/$Al_xGa_{1-x}As$ structures. (m^*, m_0, and ε_0 are the effective mass of electron, the rest mass of electron, and the permittivity of free space, respectively.)

		m^*/m_0[a]		$\varepsilon/\varepsilon_0$[a]	
x	ΔE_c (eV)	GaAs	$Al_xGa_{1-x}As$	GaAs	$Al_xGa_{1-x}As$
0.3	0.235[b]	0.067	0.092	13.18	12.24
0.54	0.437[c]	0.067	0.112	13.18	11.5

[a]From Ref. 25.
[b]From Ref. 23.
[c]From Ref. 26.

dependence. The donor concentration in the GaAs side (N_{DL}) is considered as $5 \times 10^{15}\,cm^{-3}$. All distances are measured from the GaAs/AlGaAs interface. The curves show a depletion region followed by an accumulation region along the depth as is usual for quantum structures. It is seen that at 300 K when the doping is lower ($N_{DH} = 2 \times 10^{16}\,cm^{-3}$), the peak of the ACD is as much as 29 nm away from the interface. As the doping increases, the peak gradually moves towards the interface and at the doping of $10^{18}\,cm^{-3}$ the peak is 9 nm away from the interface; whereas the peak of the actual carrier distribution moves from 8 nm to 3.6 nm for the dopings mentioned. Hence, there is a large reduction in the error at the higher doping. It is also observed that the concentration of the peak is higher than the barrier at low doping but at higher doping it is less. It should be noted that the Debye length in the barrier and in the accumulation region changes widely with the doping concentration. This causes significant change in the ACD peaks as depicted in Fig. 1.

At 50 K, the Debye smearing at different reverse bias, used in the *C-V* measurement, decreases leading to significant reduction in the shift of the carrier peaks as reflected in Fig. 1.[17] At this temperature, the large enhancement of the peak concentration as seen in the figure arises mainly due to the avoidance of quantum mechanical aspects and temperature dependence in the procedure of conventional *C-V* profiling as discussed in our published work.[17]

The error in *C-V* profiling is considered to be the deviation from the actual carrier peak, both in the position and concentration. In Fig. 2, we have plotted the errors in the concentration and position of the ACD peak with respect to the actual carrier peak due to the variation of doping concentration in $Al_xGa_{1-x}As$ for two different conduction band offsets, 0.235 eV and 0.437 eV corresponding to the Al mole fraction 0.3 and 0.54, respectively, at 300 K. It is seen that the peak concentration of ACDs may be less than or greater than the actual values. The error is defined as negative for the former case and positive for the latter. As seen in the figure, the error in the peak position decreases with higher doping, whereas error in the peak concentration increases with doping. For the higher band offset, the increase in the doping concentration raises the error of the peak concentration more sharply changing it from negative to positive, whereas it decreases the error of peak position more rapidly.

It seems from the results that for a set of parameters, it might be possible to estimate the error in the ACD for necessary corrections in the measurement. It should be noted that

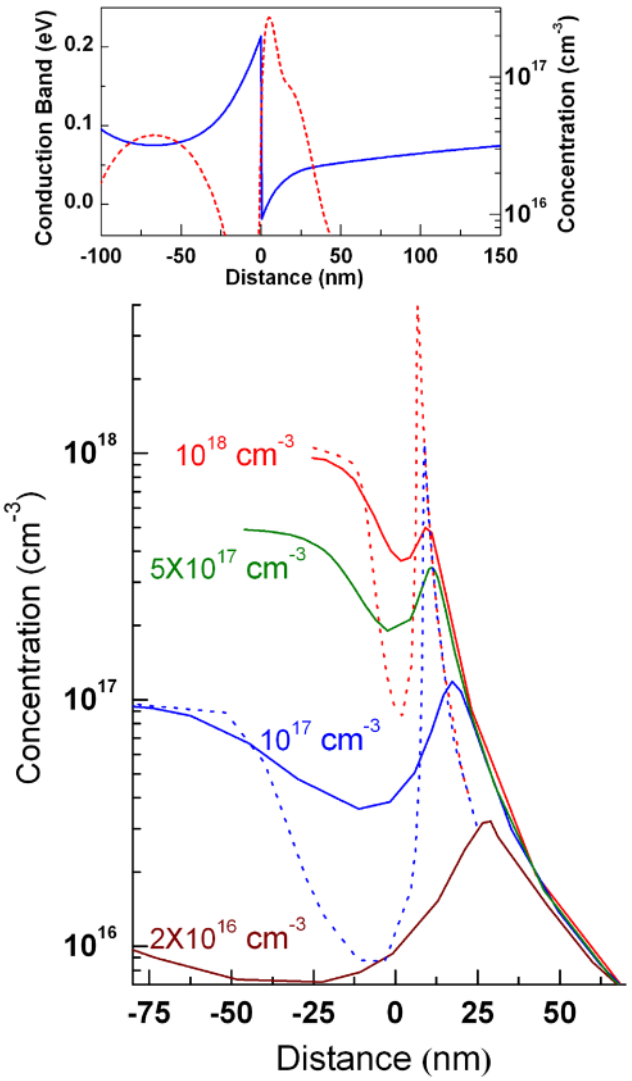

FIG. 1. ACDs in GaAs/$Al_{0.3}Ga_{0.7}As$ heterojunctions for different donor concentrations in the AlGaAs region at 300 K (solid lines) and 50 K (dotted lines) with $N_{DL} = 5 \times 10^{15}\,cm^{-3}$ and $\Delta E_c = 0.235$ eV. Inset shows the conduction band and the actual carrier distribution in a GaAs/$Al_{0.3}Ga_{0.7}As$ heterojunction for a typical case with temperature 300 K, $V_a = 0$, $N_{DH} = 10^{17}\,cm^{-3}$, $N_{DL} = 5 \times 10^{15}\,cm^{-3}$, and $\Delta E_c = 0.235$ eV. Distances are measured from the hetero-interface.

it is quite hard to formulate any analytical relation between the actual carrier distribution and the ACD since several mechanisms are responsible for the difference between the two, such as Debye smearing of 2D and 3D carriers,[19] noninclusion of quantum properties and temperature dependence in the formulation of *C-V* method,[17] the shift of the probability function with external voltage, and the effect of the series resistance of the system on the measured capacitance.[17] Except the series resistance, all of these are taken into account in our calculations.

Fig. 3 shows the variation of the peak shift and peak carrier concentration with the doping concentration at 50 K. It is seen that at low temperature the peak moves towards the interface and saturates, whereas the peak concentration increases monotonically with the doping concentration.

From all the above discussions, it is evident that by the widely used conventional computation for the extraction of

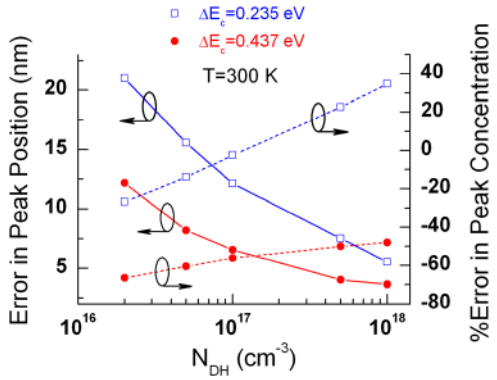

FIG. 2. Errors in the positions (solid lines) and in the concentrations (dashed line) of ACD peaks in GaAs/$Al_xGa_{1-x}As$ heterojunctions as a function of donor concentration in the AlGaAs side for two different band offsets at 300 K.

carrier profiles from C-V measurements, it is quite difficult to harness or predict the large error of measurements. Here, we are introducing a new method for computation of the carrier profile from the measured C-V data, which should be more accurate than the conventional one. Fig. 4(a) shows the experimental C-V characteristics, obtained from C-V measurements on an $In_{0.24}Ga_{0.76}As$/GaAs single QW structure with the well width 8 nm at two different temperatures. The details of the growth condition, structure, and measurements are discussed in Ref. 24. If the $1/C^2$ curve is followed for various applied reverse bias V_r, it is seen that initially it is a straight line of a finite slope and once it enters the depletion region the slope increases and as it meets the accumulation region in the QW, the slope turns to a flatter one corresponding to accumulations. In the accumulation region, the QW gets continuously depleted with increasing voltage and the curve remains almost flat and at the end of depletion it turns again for an enhanced slope. The total charge content of the QW (Q_w) is found from the region between the turning points on the $1/C^2$–V curves and is directly calculated for the accumulation region of the experimental curve as

$$Q_w = \sum_i C_i \Delta V, \tag{12}$$

where ΔV is the small voltage increments and C_i is the corresponding capacitances. The two dimensional carrier concentration (n_{2D}) is calculated as

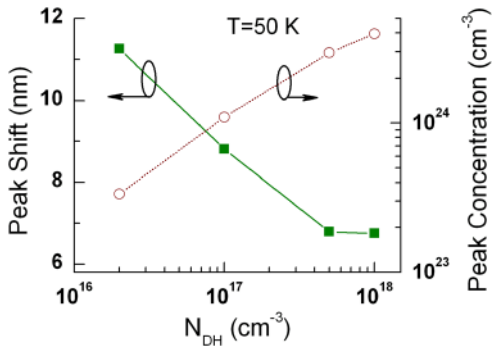

FIG. 3. The peak concentration (dotted line) and shift of peak position from the interface (solid lines) in the ACD as a function of donor concentration in AlGaAs at 50 K with $N_{DL} = 5 \times 10^{15}$ cm^{-3} and $\Delta E_c = 0.235$ eV.

$$n_{2D} = \frac{Q_w}{qA}, \tag{13}$$

where q is the electron charge and A is the area of the Schottky interface. So, using this method n_{2D} can be determined experimentally. In a narrow QW where the carriers are mostly bunched up in the first sub-band, the distribution of the confined carrier concentration can be expressed as[15]

$$n = n_{2D}|\psi_1|^2, \tag{14}$$

where ψ_1 is the normalized wave function of the carrier. For a narrow QW, ψ_1 can be approximated with that of a finite square well and determined by solving the one dimensional Schrödinger equation numerically. The method should be more effective at lower temperatures. The distance of the QW from the Schottky can be estimated as

$$d = \frac{1}{qAN_D}\left(Q_t - \frac{Q_w}{2}\right) + W, \tag{15}$$

where N_D is the doping concentration, W is the depletion width of the Schottky junction without any external bias, and Q_t is the total charge depleted from the Schottky side barrier and the QW by the external reverse bias. Q_t is calculated by integrating the C-V curve as mentioned earlier up to the second turning point.

The carrier profiles inside the QW, determined by this method, at 249 K and 9 K are shown in Fig. 4(c) along with the actual carrier profiles. The distances are measured from the Schottky. The curves match within 2% error. The carrier distributions, deduced by the conventional C-V technique, are depicted in Fig. 4(b). It is seen that the error in our developed model is almost negligible comparing to the conventional C-V carrier profiles which are, as discussed previously, widely different from the actual profiles in all respects.

The procedure can be used for a heterojunction in a similar way. In this case, the QW is approximated as an asymmetric triangular QW and d is modified as

$$d = \frac{1}{qAN_D}(Q_t - Q_w) + W, \tag{16}$$

since the depletion region exists in one side of the heterointerface.

For QWs and heterojunctions, due to very large difference between the experimental C-V carrier profiles and the actual carrier distributions, usually the C-V characteristics and the corresponding ACDs are deduced theoretically to compare with the experimental ACDs.[15,19] It is observed that at lower temperature the peak of the theoretical ACD shifts towards the Schottky, whereas for the experimental ACD, the peak shifts much away from the Schottky.[17] In our present work, similar temperature dependent shifts are observed for the GaAs/AlGaAs heterojunction and the InGaAs/GaAs QW. The shift of the peak position in the theoretical ACD can be explained by the temperature dependence of the Debye smearing of 2D and 3D electrons. The opposite shift of the ACD peak, obtained from the experiment, seems to

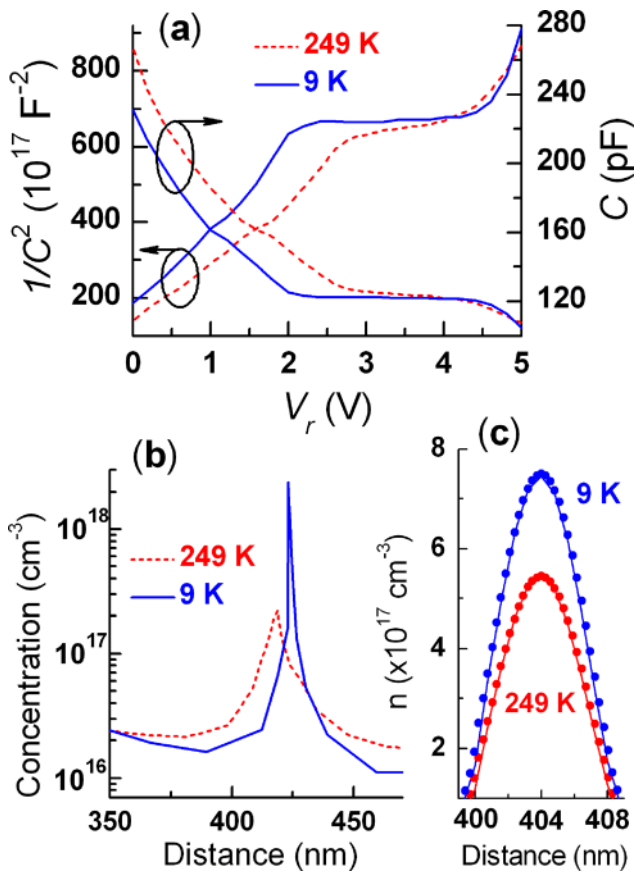

FIG. 4. (a) Experimental *C-V* characteristics of an $In_{0.24}Ga_{0.76}As/GaAs$ single QW structure at two widely different temperatures, (b) the ACDs, constructed from these *C-V* data using the conventional method, and (c) the carrier profiles, constructed from these *C-V* data, inside the QW using the modified technique (solid circles) and the corresponding actual carrier profiles (solid lines). Distances are measured from the Schottky.

arise from the temperature dependence of the series resistance across the structure. At low temperature, this series resistance increases due to several mechanisms causing large shift of the measured carrier peak. The detailed discussion is available in Ref. 17. So, to minimize the error due to series resistance it should be kept as low as possible.

IV. CONCLUSIONS

In conclusion, the ACDs obtained from *C-V* measurements on heterostructures and QWs are widely different from the actual carrier distributions, calculated from the fundamental parameters, due to errors arising from several mechanisms. We have investigated theoretically the errors in the ACD of the $GaAs/Al_xGa_{1-x}As$ heterostructure with doping concentration for different band offsets and temperatures. The study will be helpful to estimate the errors in the position and concentration of the ACD peak, obtained from the measurement, in a particular heterostructure at a particular temperature. It is observed that the error in the peak position decreases at higher doping, higher band offset, and lower temperature, whereas the error in the peak concentration has a complex response with the parameters. To minimize the error, we have described a modified technique for determination of the carrier profile of a nanostructure more accurately than the conventional one from the measured *C-V* data.

ACKNOWLEDGMENTS

One of the authors (S.P.) acknowledges the financial support from the University Grants Commission, Government of India under the RFSMS scheme.

[1]G. T. Du, W. Zhao, G. G. Wu, Z. F. Shi, X. C. Xia, Y. Liu, H. W. Liang, X. Dong, Y. Ma, and B. L. Zhang, Appl. Phys. Lett. **101**, 053503 (2012).
[2]G. G. Wu, W. C. Li, C. S. Shen, F. B. Gao, H. W. Liang, H. Wang, L. J. Song, and G. T. Du, Appl. Phys. Lett. **100**, 103504 (2012).
[3]D. Shao, M. Yu, J. Lian, and S. Sawyer, Appl. Phys. Lett. **101**, 211103 (2012).
[4]R. S. Crandall, E. Iwaniczko, J. V. Li, and M. R. Page, J. Appl. Phys. **112**, 093713 (2012).
[5]T. Hofmann, P. Kuhne, S. Schoche, Jr-T. Chen, U. Forsberg, E. Janzen, N. Ben Sedrine, C. M. Herzinger, J. A. Woollam, M. Schubert, and V. Darakchieva, Appl. Phys. Lett. **101**, 192102 (2012).
[6]C. C. Tang, M. Y. Li, L. J. Li, C. C. Chi, and J. C. Chen, Appl. Phys. Lett. **101**, 202104 (2012).
[7]H. Khmissi, M. Baira, L. Sfaxi, L. Bouzaiene, F. Saidi, C. Bru-Chevallier, and H. Maaref, J. Appl. Phys. **109**, 054316 (2011).
[8]P. Kamyczek, E. Placzek-Popko, Vl. Kolkovsky, S. Grzanka, and R. Czernecki, J. Appl. Phys. **111**, 113105 (2012).
[9]Y. S. Park, M. Lee, K. Jeon, I. T. Yoon, Y. Shon, H. Im, C. J. Park, H. Y. Cho, and M. S. Han, Appl. Phys. Lett. **97**, 112110 (2010).
[10]Z.-Q. Fang, D. C. Look, D. H. Kim, and I. Adesida, Appl. Phys. Lett. **87**, 182115 (2005).
[11]H. Kroemer, W. Y. Chien, J. S. Harris, Jr., and D. D. Edwall, Appl. Phys. Lett. **36**, 295 (1980).
[12]S. D. Kwon, H. Lim, H. K. Shin, and B. D. Choe, Appl. Phys. Lett. **69**, 2740 (1996).
[13]M. O. Watanabe, J. Yoshida, M. Mashita, T. Nakanisi, and A. Hojo, J. Appl. Phys. **57**, 5340 (1985).
[14]L. Jia, E. T. Yu, D. Keogh, P. M. Asbeck, P. Miraglia, A. Roskowski, and R. F. Davis, Appl. Phys. Lett. **79**, 2916 (2001).
[15]V. I. Zubkov, M. A. Melnik, A. V. Solomonov, E. O. Tsvelev, F. Bugge, M. Weyers, and G. Tränkle, Phys. Rev. B **70**, 075312 (2004).
[16]S. Panda and D. Biswas, J. Appl. Phys. **108**, 066104 (2010).
[17]S. Panda and D. Biswas, J. Appl. Phys. **109**, 056102 (2011).
[18]S. Panda and D. Biswas, Mater. Sci. Semicond. Process. **16**, 1090 (2013).
[19]C. R. Moon, B. D. Choe, S. D. Kwon, and H. Lim, Appl. Phys. Lett. **72**, 1196 (1998).
[20]I.-H. Tan, G. L. Snider, L. D. Chang, and E. L. Hu, J. Appl. Phys. **68**, 4071 (1990).
[21]W. H. Press, S. A. Teukolsky, W. T. Vetterling, and B. P. Flanery, *Numerical Recipes: The Art of Scientific Computing*, 3rd ed. (Cambridge University Press, New York, 2007).
[22]J. L. Thobel, L. Baudry, P. Bourel, F. Dessenne, and M. Charef, J. Appl. Phys. **74**, 6274 (1993).
[23]D. Kim, J. Khang, and A. Madhukar, J. Korean Phys. Soc. **23**, 397 (1990).
[24]D. Biswas, S. Chakrabarti, S. Dasgupta, S. Kundu, and R. Datta, Phys. Status Solidi B **236**, 55 (2003).
[25]S. Adachi, J. Appl. Phys. **58**, R1 (1985).
[26]D. Arnold, A. Ketterson, T. Henderson, J. Klem, and H. Morkoç, Appl. Phys. Lett. **45**, 1237 (1984).